High Resolution Mapping of Thermospheric Wind and Temperature

M. Conde,[1] C. Anderson[1] T. Davies,[2] P. Dyson,[2] M. Kosch,[3] [[1]Geophysical Institute, UAF; [2]LaTrobe University; [3]Lancaster University]

Abstract

All-sky imaging Fabry-Perot spectrometers can provide two dimensional maps of thermospheric wind and temperature fields over a circular region spanning around 1400 km in diameter at F-region heights, or about half this in the E-region. Typical configurations used to date have resolved a few tens of look directions across their field of view. Here we report on an 8-day campaign conducted in March of 2011 in which an instrument at Mawson, Antarctica, was configured to resolve its wind and temperature measurements into 261 independent look directions. This is far higher spatial resolution than has ever been attempted previously. It was made possible by the combination of a new and more sensitive detector coupled with observations taken during a period of higher solar and magnetic activity than has been typical in recent years. Several nights of excellent data were obtained during the campaign; here we show examples from March 11. Spatial variations in the wind field are well resolved at this zone density, and the 5577 Å Doppler temperature fields resolve a lot of structure associated with individual auroral arcs. While this mode is probably not optimum during periods of weak signal, it is does work well during active times. An important application would be to improve the density of bistatic or tristatic wind measurements

Introduction

In the mid 1990's the University of Alaska's Geophysical Institute developed a new type of Fabry-Perot spectrometer for remote sensing thermospheric wind and temperature fields. Installed at Poker Flat in Alaska and dubbed the "Scanning Doppler Imager", its salient features included a low-light imaging detector with high time resolution, a capacitance-stabilized etalon capable of piezo-electric separation scanning at 10 Hz or faster, and wide-angle fore optics arranged to place a sharp image of the sky onto the detector [*Conde & Smith*, 1995, 1997, 1998; *Conde et al.* 2001]. With appropriate calibration data and real-time image processing, the instrument can resolve the sky scene into a software-defined set of sub-regions (known as "zones"), and compile a high-resolution Doppler spectrum of the source illumination originating from each zone.

Doppler shifts and Doppler widths of the various spectra across the field of view are then used to infer two-dimensional maps of vector wind and scalar temperature at the height of the atmospheric optical emission layer. Division of the field-of-view into zones is done using a lookup table known as a "zone map". This provides great flexibility – in principle, any number of zones can be defined, and they could have any shape. However, for a given configuration of optical hardware there is an upper limit on the number of useful zones, that is imposed by the inevitable trade-off between resolution and sensitivity. As more zones are allocated, each zone "receives" a smaller fraction of the total photon flux collected by the instrument. Thus, the only way to increase the number of viable zones is to make the instrumental hardware itself more sensitive.

Even the original mid-1990's version of this instrument achieved an optical etendue that was within a factor of two or so of the best possible today. So there has been little scope for improvement through installing a larger aperture etalon or bigger lenses. However, there has been a steady and substantial improvement in detector performance in the last 15 years. The combination of these better detectors and gradual improvements in signal processing have produced more than an order of magnitude improvement in the overall sensitivity of this and subsequent instruments relative to the original version. This improvement is illustrated below, where representative spectra are shown overlaid onto the fields of wind, temperature, and emission brightness that were derived from them.

The Mawson Instrument

In 2006 a second scanning Doppler imager was constructed by LaTrobe University in Australia, in collaboration with Lancaster University in the UK. The instrument is illustrated opposite. Its optics provide about twice the etendue of the one at Poker Flat. But much more importantly, it was the first such instrument to use an EMCCD detector, which was a huge advance over the intensified CCD system being used in Alaska at that time. In early 2007 it was installed at Mawson, Antarctica, where it ran until early 2009, when the EMCCD camera failed. No data were acquired during the 2009 or 2010 austral winter seasons. A new camera was installed in January 2011, so that the instrument is now running again and collecting excellent data.

With the latest camera and higher solar activity, the refurbished Mawson SDI is more sensitive than ever. Thus, we decided in March of 2011 to try a few days observations using a very high density zone map, with 261 zones allocated. The campaign ran for 8 days, of which there were about 4 days of good seeing and active aurora. Here we present a few examples from one such day.

The Mawson Scanning Doppler Imager being tested at LaTrobe University in 2006, prior to shipment to Antarctica.

Temperatures

The figure below here shows sky maps of Doppler temperature inferred from the 557.7 nm emission. Most of the 557.7 nm signal recorded here was excited by auroral precipitation. The height of the aurorally-excited emission layer is strongly dependent on the characteristic energy of the auroral precipitation – harder precipitation penetrates deeper into the E-region, and excites 557.7 nm emission from lower altitudes. Because of the large vertical temperature gradient, the resulting Doppler temperature is mostly an indication of the characteristic energy of the precipitation (although there are some smaller heating effects as well.) The figure below is thus a two dimensional map of this precipitation energy. While we have been able to produce such maps for a number of years, we can now achieve far higher spatial resolution.

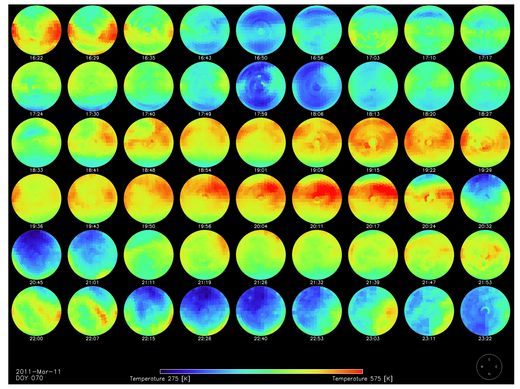

Sky maps of 557.7 nm Doppler temperature recorded on March 11, 2011. Red hues indicate higher temperatures, corresponding to emission coming from higher in the atmosphere than from the regions depicted with blue hues.

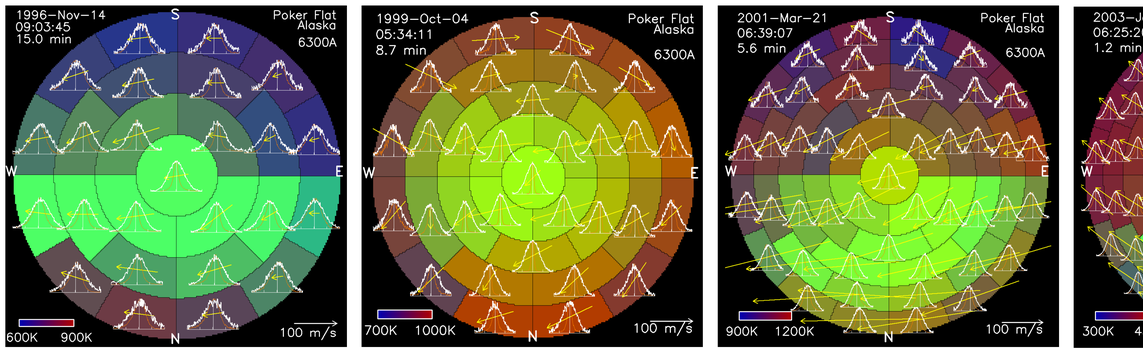

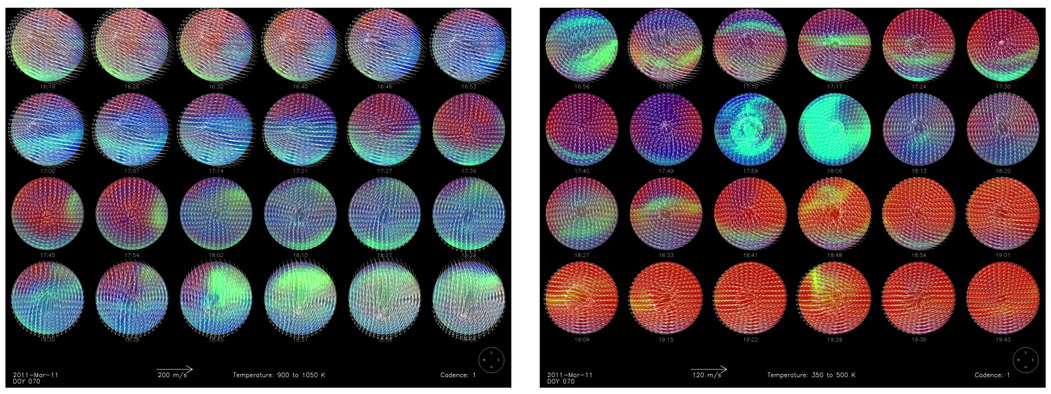

Two dimensional vector wind fields derived from Doppler shifts of the 630 nm emission (left) and the 557.7 nm emission (right) during the first part of evening of March 11, 2011. Background blue through red hues depict Doppler temperature over the range indicated on the plots. Green hues depict emission brightness obtained from summing all fringe images, as described in the text.

Winds

The two figures opposite are examples of the horizontal wind fields obtained during the high-resolution campaign. The left panel shows winds derived at F-region heights of around 240 km using the 630 nm emission. The right panel shows winds at E-region heights of 110 km to 140 km derived from the 557.7 nm emission. Vector fields were fitted to line-of-sight winds using the method described by *Conde & Smith* [1998]. Background blue through red hues depict Doppler temperature, whereas green hues depict emission brightness.

The emission brightness images shown here (and in the right-most three panels of the historical sequence shown above) were obtained by co-adding all camera images recorded during a single "exposure". At any given instant, the camera sees an all-sky view of the emission brightness, modulated by a Fabry-Perot ring pattern. By co-adding all such images as the etalon scans, the Fabry-Perot modulation is averaged out, leaving just the brightness distribution of the original sky scene. Although a separate all-sky camera could easily achieve higher temporal and spatial resolution, the all-sky images obtained by the instrument itself correspond to exactly the same field-of-view and time interval as that used to acquire the spectra.

The F-region wind fields shown here are relatively uniform. However, the wind direction shifted by around 90° during the 45 min between 17:15 and 18:00 UT, and the maps here show how this occurred – a line of shear swept from south to north across the field of view. The shear is easily seen in the panels for times from 17:27 to 17:45.

Much more variability is evident in the 558 nm wind fields. While the actual wind field likely does contain more structure at E-region heights, there are also artifacts in the 558 nm Fabry-Perot data. It is well known that the E-region contains large vertical wind shears. As is apparent from the temperature plot above, the height of the 558 nm emission could vary by as much as 10 or 20 km across the field of view. In the presence of vertical shear, this would introduce changes in line of sight wind across the field of view that would be incorrectly interpreted as horizontal structure. Further, artifacts can arise in the SDI spectra if the emission brightness varies rapidly with time – which it clearly did do during these observations.. Nevertheless, even though these artifacts do occur quite frequently, it is also surprising how often the 558 nm data are well behaved.

Deriving horizontal vector winds from a single observatory is based on a Fourier decomposition (up to $m = 2$) of line-of-sight wind speed versus viewing azimuth. Because the cosine function only varies slowly in azimuth, not all of the variability present in the wind fields will be resolved by the monostatic analysis, regardless of how many zones are allocated. However, we are currently moving to bistatic and soon tristatic observations, which will make full use of every additional zone that we can allocate.

References

Conde, M., and R. W. Smith (1995), Mapping thermospheric winds in the auroral zone, *Geophysical Research Letters*, 22, 3019-3022.

Conde, M. and R. Smith (1997), Phase compensation of a separation scanned, all-sky imaging Fabry-Pérot spectrometer for auroral studies, *Appl. Opt.*, 36, 5441-5450.

Conde, M., and R. W. Smith (1998), Spatial structure in the thermospheric horizontal wind above Poker Flat, Alaska, during solar minimum, *Journal of Geophysical Research*, 103, 9449-9471.

Conde, Crawen, Immel, Hoch, Stenbaek-Nielsen, Hallinan, Smith, Olson, Wei Sun, Frank, and Sigwarth, (2001), Assimilated observations of thermospheric winds, the aurora, and ionospheric currents over Alaska, *J. Geophys. Res.* 106:10493-10508.